Dipole Dynamics and Macroscopic Alignment in Molecular and Polymeric Liquid Crystals by Broad-Band Dielectric Relaxation Spectroscopy

Jovan Mijovic* and Jo-Wing Sy

Department of Chemical Enginering and Chemistry and The Herman F. Mark Polymer Research Institute, Polytechnic University, Six Metrotech Center, Brooklyn, New York 11201

Received August 11, 2000; Revised Manuscript Received October 24, 2000

ABSTRACT: A liquid crystal monomer (LCM) was synthesized and attached as a side chain to a siloxane polymer (SCLCP). The molecular dynamics of LCM and SCLCP were investigated by broad-band dielectric relaxation spectroscopy (DRS) over 10 decades of frequency. The surface treatment of the electrodes was found to have a pronounced effect on the macroscopic alignment and dynamics. In the isotropic state the relaxations in LCM and SCLCP are well-described by the Kohlrausch−Williams−Watts (KWW) functional form. In the LC state, the overall dielectric response is a weighted sum of two dispersions that depend on the macroscopic alignment. The hometropic (H) alignment is dominated by the (slower) δ process, while the planar (P) alignment is dominated by the (faster) α_m process. Both processes are symmetric and can be described by Cole−Cole (CC) or Fuoss−Kirkwood (FK) functional forms. The δ process governs the dynamics in the SCLCP near the glass transition, similar to the segmental α process in non-LC glass formers. Excellent agreement was observed with the various aspects of the seminal work by Attard and Williams.

Introduction

The molecular dynamics of liquid crystal (LC) molecules are complex,[1−7] and our understanding of the reorientational motions in these anisotropic systems over a broad range of temperature and frequency remains incomplete despite a number of experimental and theoretical investigations.

A variety of experimental methods have been used to identify and characterize the structure and phase behavior of LC materials, including differential scanning calorimetry (DSC), optical microscopy (OM), X-ray diffraction, neutron scattering, fluorescence depolarization, dynamic mechanical analysis (DMA), thermomechanical analysis (TMA), and dielectric relaxation spectroscopy (DRS). Of these methods, broad-band DRS is particularly suitable for the study of reorientational dynamics. The great attraction of DRS derives from an unparalleled frequency range available (up to 16 decades) that enables one to conduct fundamental studies of molecular dynamics of condensed matter in various phases and at different temperatures: from amorphous liquids to liquid crystals to an amorphous or crystalline glass; from high temperature, where the dipole relaxation times are of the order of tens of picoseconds, through the vitrification process where relaxation times in the glassy state reach tens to hundreds of seconds. There is also a strong practical motivation for the study of dynamics by DRS: consider, for example, that electric field-induced switching of LC displays is rooted in the anisotropy of the dielectric permittivity—the principal parameter measured by DRS. The theoretical treatment of the dielectric response of monodomain and polydomain LCs is given in the literature,[8−12] and only its salient features of direct relevance to this work are recapped below.

* To whom correspondence should be addressed.

Theoretical Background

Relationship between dielectric permittivity and the dipole moment correlation function for isotropic amorphous systems[13−15] can be generalized further to account for anisotropic LC systems, as described in seminal contributions by Williams, Attard, and co-workers.[8−12] For the simple case where the internal field factors are set to unity, two principal complex permittivities, $\epsilon_{||}(\omega)$ and $\epsilon_{\perp}(\omega)$, in an axially symmetric LC phase are written as

$$\frac{\epsilon_\gamma(\omega) - \epsilon_{\infty\gamma}}{\epsilon_{0\gamma} - \epsilon_{\infty\gamma}} = 1 - i\omega F\,[\Phi_{\mu\gamma}(t)] \tag{1}$$

$$[\Phi_{\mu\gamma}(t)] = \frac{\langle \mu_{k\gamma}(0)\,\mu_{k\gamma}(t)\rangle}{\langle \mu_{k\mu}^2\rangle} \tag{2}$$

where $\gamma = ||$ or $\perp$. The two permittivities, $\epsilon_{||}(\omega)$ and $\epsilon_{\perp}(\omega)$, are measured parallel and perpendicular to the principal axis, respectively. For simplicity, only the autocorrelation terms are included in eq 2, although cross-correlation terms can be readily introduced formally for an LC.[12] The form that the correlation function takes in an LC depends on the macroscopic alignment of the sample. Araki et al.[10] have developed a general relationship between the principal complex permittivities and the correlation function for the dipole motion, shown in eqs 3 and 4:

$$\epsilon_{||}(\omega) = \epsilon_{\infty||} + \frac{G}{3kT}[(1 + 2S)\mu_l^{\,2}\,F_{||}^{l}(\omega) + (1 - S)\mu_t^{\,2}\,F_{||}^{t}(\omega)] \tag{3}$$

$$\epsilon_{\perp}(\omega) = \epsilon_{\infty\perp} + \frac{G}{3kT}[(1 + 2S)\mu_l^{\,2}F_{\perp}^{l}(\omega) + (1 - S/2)\mu_t^{\,2}F_{\perp}^{t}(\omega)] \tag{4}$$

10.1021/ma0014158 CCC: $19.00
Published on Web 12/02/2000

In eqs 3 and 4, μ_l and μ_t are the longitudinal and transverse dipole moments in the mesogens, respectively; G is a term involving the concentration of dipolar mesogenic group; S is the local order parameter and the Fourier transform relation gives F:

$$F_j^i(\omega) = 1 - i\omega F\,[F_j^i(t)] \tag{5}$$

The measured permittivity along the direction of the electric field (Z-direction) in an (arbitrarily) macroscopically aligned sample is written as[9]

$$\epsilon_Z(\omega) = \left(\frac{1 + 2S_d}{3}\right)\epsilon_{||}(\omega) + \frac{2}{3}(1 - S_d)\epsilon_{\perp}(\omega) \tag{6}$$

$$S_d = \langle 3\cos^2\theta_{nZ} - 1\rangle/2 \tag{7}$$

where S_d is the macroscopic director order parameter and θ_{nZ} is the angle between the director axis and the measuring field direction. S_d is equal to 0, 1.0, and -0.5 for an unaligned, fully H-aligned, and fully P-aligned, respectively. The permittivity in an arbitrarily aligned sample is a weighted sum of the four relaxation modes (two involve $\mu_{||}$, 00, 10 and two involve $\mu_{\perp}$, 01, 11). The $F_{||}^l(\omega)$ region (00) is believed to be associated with the end-over-end reorientation of the long molecular axis and appears at lower frequency due to the nematic potential barrier.[16] This relaxation is often referred as the δ process and is specific to the mesophase. The $F_{||}^t(\omega)$ (01) region is related to the fast rotation of molecule along its long axis, which also fluctuates about the director over a limited solid angle on a similar time scale. $F_{\perp}^l(\omega)$ (10) and $F_{\perp}^t(\omega)$ (11) involve fast rotations of a molecule about the long axis and fluctuations in a small angle about the director. Taking relaxation in the isotropic state as a reference, $F_{||}^l(\omega)$ should be significantly slower than $F_{||}^t(\omega)$, $F_{\perp}^l(\omega)$, and $F_{\perp}^t(\omega)$. In fact, it was shown by Nordio[17] that the average relaxation times τ_{ij} for small-step diffusion in the nematic potential is as follows: $\tau_{00} > \tau_{01} \geq \tau_{11} \geq \tau_{10}$.

The dipole moment correlation function in isotropic systems is most often quantified via a stretched exponential function of the Kohlrausch−Williams−Watts[18] (KWW) type. The relaxation spectra in the LC phase, however, are more symmetric, and the Fuoss−Kirkwood (FK) empirical function is often used instead. The relaxation kernel can be also evaluated from the real or imaginary (they are related by the Kramers−Kronig transform) portion of the measured permittivity. In this study, however, instead of transforming the frequency domain dielectric data into the time domain using a discrete Fourier transform, where spectral features may be truncated, we transform the relaxation kernel into the frequency domain, following Dishon et al.[19] Alternatively, ϵ^* may be modeled by an empirical functions in the frequency domain; a particularly popular and robust form is the Havriliak−Negami[20] (HN) function, which was employed here with an additional conductivity term.

The principal objectives of this study are (1) to contrast the dynamics of LC monomer (LCM) and side-chain LC polymer (SCLCP) over 10 decades of frequency, (2) to investigate the effect of surface treatment on the alignment and the dielectric response of LCM and SCLCP, and (3) to compare the temperature dependence of relaxation processes in LC and non-LC glass formers.

Experimental Section

Materials. LCM (**3**) was synthesized by reacting 4′-hydroxy-4-biphenylcarbonitrile (**1**) and ω-alkenyl bromide (**2**). Both compounds were supplied by Aldrich Chemical Co. SCLCP (**5**) was prepared by reacting the LCM (**3**) with poly(hydrogen methylsiloxane) (**4**), obtained from United Chemical Technologies Inc., with average molecular weight, M_n = 4000 g/mol. The synthesis was onducted according to the published procedure.[21−23] The product (**5**) was dried at 45 °C under vacuum for 1 week to remove the residual solvent prior to measurements.

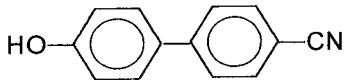

(1)

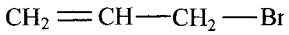

(2)

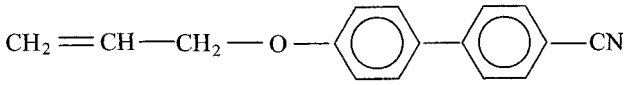

(3)

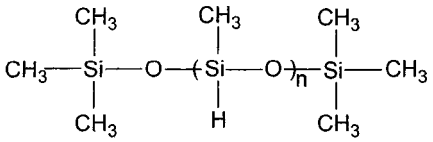

(4)

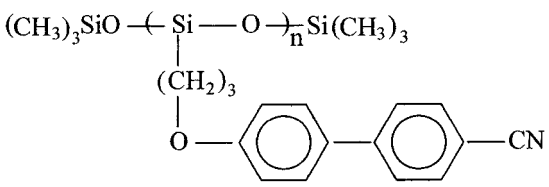

(5)

Techniques. The principal experimental tool that we have used is broad-band dielectric relaxation spectroscopy (DRS). Of the experimental techniques available for the study of relaxation processes in polymeric and molecular glass formers, DRS is rapidly becoming a dominant tool.[24−27] A more detailed description of our experimental facility for dielectric measurements is given elsewhere,[28,29] and several excellent reviews of experimental methodology for dielectric measurements were recently published.[30−32] However, briefly, we have used Solarton 1260 impedance gain phase analyzer (10 μHz−32 MHz) with broad-band dielectric converter (Novocontrol GmBh), Hewlett-Packard (HP) 4284 A Precision LCR meter (20 Hz−1 MHz), and Hewlett-Packard 4291 A RF impedance analyzer (1 MHz−1.8 GHz). All instruments are interfaced to computers via IEEE 488.2 and are equipped with heating/cooling capabilities, including Novocontrol's Novocool system. Parallel plate configuration was used, and the sample thickness was 50 μm. Supporting evidence was obtained from Fourier transform infrared (FTIR) spectroscopy, using Nicolet Instrument's Magna 750 spectrometer as described elsewhere,[33] differential scanning calorimetry (DSC), using TA instrument DSC model 2920 at a heating rate of 10 °C/min, and optical microscopy (OM) using a Nikon HFX-II optical microscope.

As will be made amply clear in the text, the surface treatment of the electrodes used for dielectric measurement is of crucial importance. Two different types of surfaces were

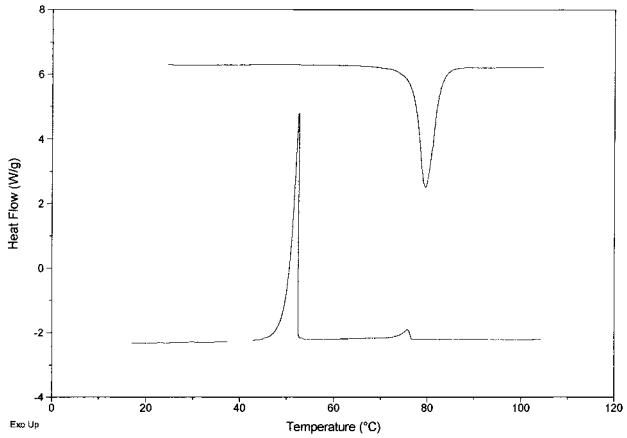

Figure 1. DSC thermograms of LCM.

used: (1) clean polished copper surfaces and (2) polyimide-(PI)-coated surfaces. The latter were prepared as follows: poly-(3,3′,4,4′-benzophenonetetracarboxylic dianhydride-*co*-4,4′-oxydianiline/1,3-phenylenediamine) amic acid solution was spin-coated onto a clean copper electrode. The coated electrodes were placed in an oven at 200 °C for 3 h, and the coated surface was rubbed with velvet prior to applying the sample. The thickness of the coated PI film was less than 1 μm, and its contribution to the measured dielectric response was considered negligible.

A final comment: in selecting the above-described LCMs and SCLCPs, we have built largely upon the earlier work by Attard, Williams, and their colleagues. There are, however, several aspects of our work that are original and noteworthy: (1) the use of a considerably broader frequency range, (2) a simultaneous study of LCM and its SCLCP, (3) the use of different (and novel) surface treatments to align samples, and (4) a direct comparison of relaxation characteristics in the isotropic and LC phase.

Results and Discussion

The presentation of our results is divided into two parts: part one focuses on the dynamics of the LCM while part two discusses the dynamics of the SCLCP.

LC Monomer (LCM) Dynamics. We begin by examining the DSC thermogram shown in Figure 1. A sharp melting peak (T_m) is observed at 80 °C during heating (upper trace). Two sharp peaks are clearly seen during cooling (lower trace); a peak at 77 °C associated with the transition from the isotropic to the nematic state (T_i = clearing temperature) and a peak at 53 °C (T_c) due to crystallization. Therefore, this LCM can be rendered liquid crystalline by cooling to a temperature between T_i and T_c.

It is well-known that the orientation in LC materials, LCMs and LC polymers (LCPs) alike, can be induced by a contact with different surfaces, and that has important implications in dielectric measurements where samples are commonly contained between two electrodes. As we shall demonstrate below, substantial homeotropic (H: $S_d = 1$), planar (P: $S_d = -0.5$), and random alignment ($S_d = 0$) can all be induced in our samples by an appropriate choice of the electrode surface.

Dielectric loss in the frequency domain with temperature as a parameter, measured using three different electrode surfaces, is shown in Figure 2A−C. Let us begin by examining Figure 2A, which was obtained using clean copper electrodes. We start at high temperature, where the material is isotropic. The data show the α process, common to all glass-formers, located at

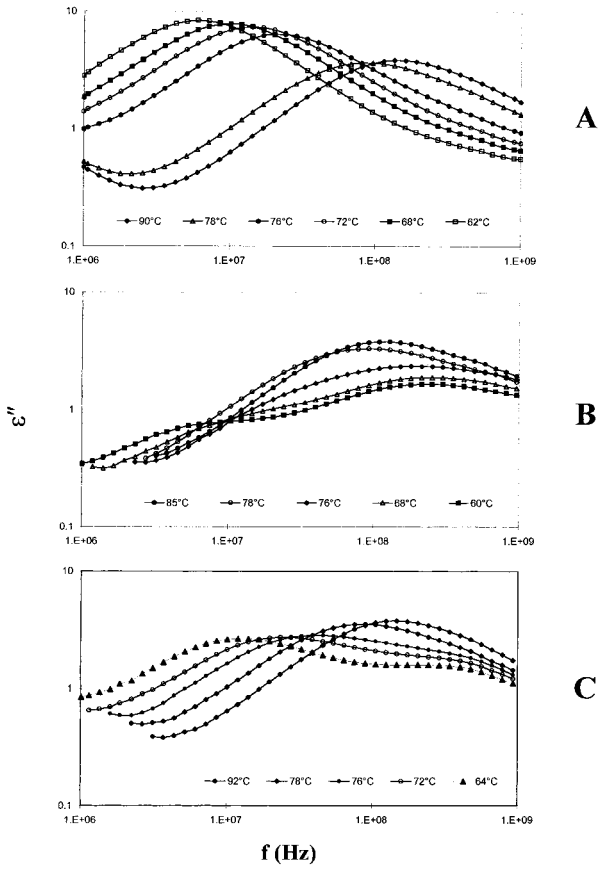

Figure 2. Dielectric loss in the frequency domain with temperature as a parameter for LCM: (A) clean copper electrodes, (B) PI-coated electrodes, (C) clean/PI-coated electrodes.

about 200 MHz at 90 °C. The α process shifts gradually to lower frequency and decreases in intensity with decreasing temperature between 90 and 78 °C. Between 78 and 76 °C, however, an abrupt change is observed; the relaxation peak shifts to lower frequency by more than half decade while its intensity increases considerably. These changes are a signature of the phase transition (I−N, isotropic to nematic), and the temperature at which this takes place is in agreement with the DCS result (T_i = 77 °C). We defer further analysis of these results until later in order to promptly emphasize the strikingly different result obtained with PI-coated electrodes, shown in Figure 2B. Actually, the behavior described in parts A and B of Figure 2 is identical *above* but vastly different *below* the isotropic to nematic transition. As the temperature is decreased below T_i, the relaxation peak (Figure 2B) shifts to *higher* frequency and decreases in strength. At still lower temperature (e.g., 60 °C), another relaxation process emerges (becomes visible) at a frequency similar to that of the peak in Figure 2A.

The observation that the dielectric response in the LC state depends strongly on the surface treatment of the electrodes suggests that a different macroscopic alignment was induced in those two cases. Before proceeding with DRS analysis, we sought supporting evidence from polarized optical microscopy (POM). Figure 3 contains a series of micrographs of our LCM obtained during the I−N transition on the clean glass surfaces (Figure 3A,B) and the PI-treated surfaces (Figure 3C−E). All samples are isotropic above 78 °C as judged by the black background observed under the polarized light. Figure

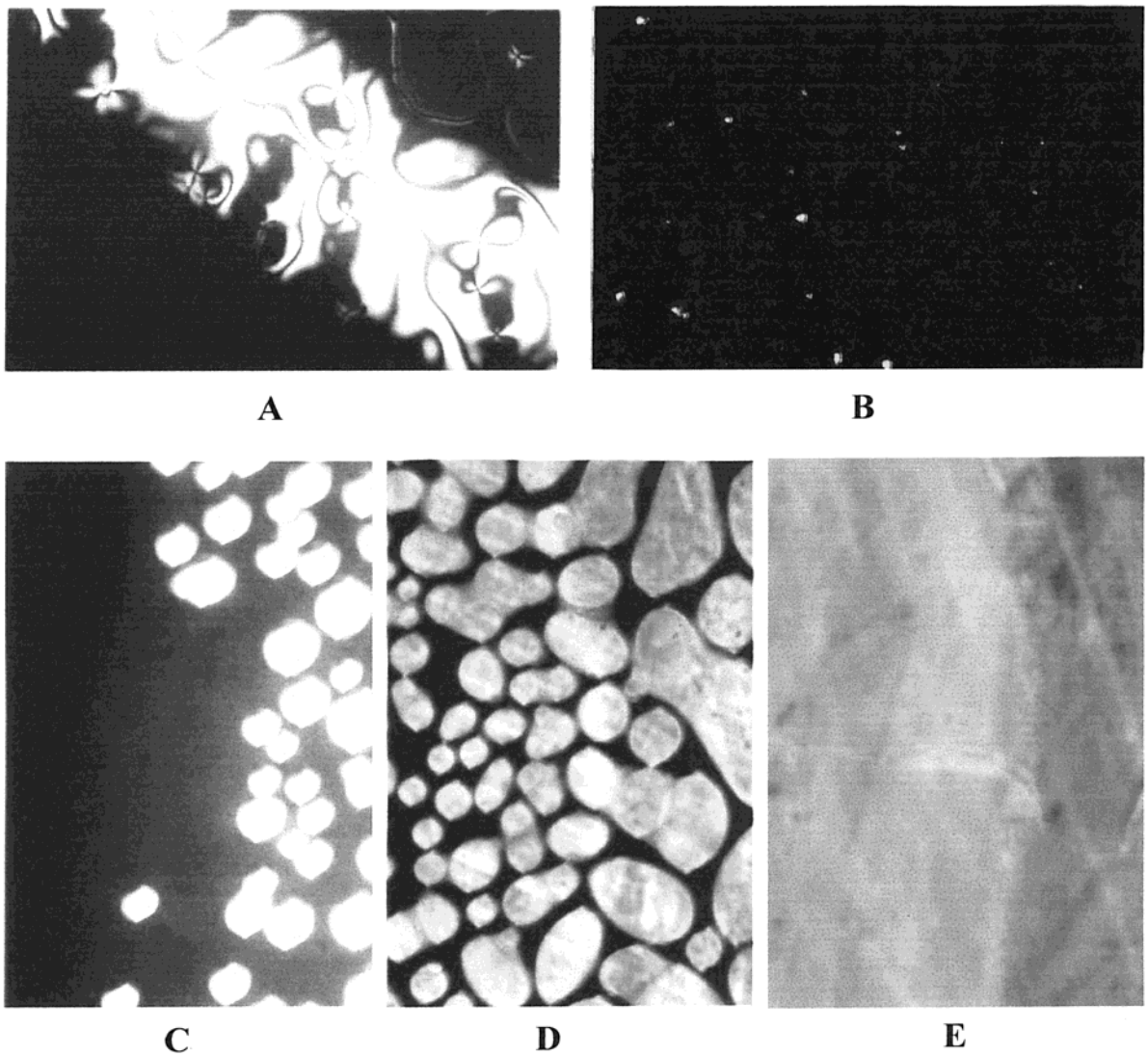

Figure 3. Polarized optical micrographs of LCM during the I−N transition: (A, B) on clean glass surfaces; (C−E) on PI-coated glass surfaces.

3A,B describes the change in texture during cooling of a sample on clean surfaces. The decrease in temperature to 76 °C is accompanied by the formation of bright droplets which are known to characterize the nematic phase of LCMs and LCPs. The micrograph shown in Figure 3A was taken during that transition, and the characteristic Schlieren pattern is clearly observed. But a few seconds later the background turns black again, and only sporadic bright spots remain visible (Figure 3B). The dark areas that reappear are a result of the spontaneous orientation in the mesophase that gives rise to the formation of a homeotropic texture. The development of a planar alignment from an isotropic mixture is shown in Figure 3C,D. The formation of bright droplets (unaligned nematic phase) from the isotropic liquid is shown in Figure 3C. Further expansion and orientation of the LC regions give rise to the texture observed in Figure 3D. Finally, a uniform planar texture is achieved (Figure 3E).

Let us now briefly contrast the measured dielectric respones with the theoretical prediction. According to eq 3, two relaxation domains should be observed in the homeotropic LC state. Figure 2A shows that two relaxations are indeed present: a stronger, slow process and a weaker, fast process (high-frequency end of Figure 2A). The slower relaxation is associated with the δ process (mode 00) while the faster relaxation is related to mode 01, in line with the earlier studies. For fully planar alignment the δ process should be absent, and the loss curve should be dominated by modes 10 and 11. We see in Figure 2B that the loss spectrum in the LC state is indeed dominated by a broad fast process. The presence of a low-frequency shoulder (clearly seen at 60 °C) is taken as indication that the sample is not completely planar. Careful inspection of the spectra of Figure 2A,B reveals similar frequency location for modes 01, 10, and 11, in further agreement with calculations of the average relaxation times for small-step diffusion in the nematic potential (eq 7). For clarity, the broad dispersion that encompasses the contributions of modes 01, 10, and 11 is termed α_m, where subscript "m" denotes mesophase.

We have established above that H and P alignments are preferred on clean and PI-treated surfaces, respectively. A question arises: what if the measurement cell is made up of one clean and one PI-treated electrode? We prepared and tested such sample, and, interestingly, discovered that the ensuing alignment was approximately random. This result is shown in Figure 2C. Two relaxations of comparable strength, δ and α_m, in as-

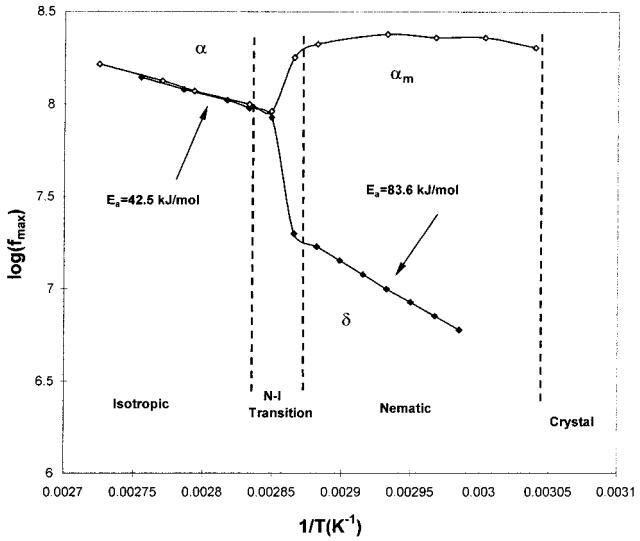

Figure 4. Frequency at maximum loss as a function of reciprocal temperature for α, α_m, and δ processes in LCM.

cending order of frequency, are clearly observed in the mesophase. Since one electrode induces H and the other P alignment, the director must make its way from one surface to the other in a continuous manner. Therefore, the director effectively splays from the vertical to horizontal on going from H to P alignment. It is apparent that the averaging over elements lying between parallel and perpendicular will give a result intermediate between H and P alignments, close to the nominally unaligned sample. However, this situation is very different from a randomly orientated polydomain for which $S_d = 0$. It is also interesting to note that the composite alignment observed in this sample cannot be realized with electric or magnetic fields since the dissimilar electrodes allow a symmetry-breaking configuration to be achieved.

The frequency of maximum loss for different relaxation processes is plotted as a function of temperature in Figure 4. The data obtained on clean surfaces (solid diamonds) and PI-tretaed surfaces (open diamonds) fall on top of each other above the T_i, indicating that the effect of surface treatment on the α process in the isotropic state is negligible. The splitting of the α process into two processes, δ and α_m, occurs in the LC state, following the I−N transition. With decreasing temperature, the α_m process shifts to higher frequency and the δ process to lower frequency. Within the temperature range of Figure 4, both α (isotropic state) and δ processes are Arrhenius, with an activation energy of 42.5 and 83.6 kJ/mol, respectively. Note that the δ process shows a much stronger temperature dependence (E_a is doubled, probably due to the interactions in the nematic phase that hinder the end-over-end reorientation). It is also interesting that the activation energies for α and δ processes fall in the range of values commonly found for the localized β relaxations (typically between 10 and 100 kJ/mol), suggesting that the molecular motions in this LCM are less cooperative.

We now examine the shape of various relaxation processes. As shown in Figure 2, only the α process is observed in the isotropic state ($T > T_i$), while two disperisons (δ, α_m) are detected in the LC state ($T_i > T > T_c$). The frequency location of modes 01, 10, and 11 was similar but, at the same time, well-separated from the δ process (mode 00). Consequently, the loss spectrum in the LC state was taken to consist of two processes, δ and α_m, and deconvolution was carried out. These results are summarized in Table 1 and are discussed next. We consider the isotropic state first. The α process is well described by the KWW function, and the loss peak becomes narrower with increasing temparture. For example, KWW β is 0.69 at 70 °C and 0.72 at 90 °C, considerably greater than the typical value for most amorphous polymers (about 0.5). We note that the motions of elongated mesogenic groups will be anisotropic even in the isotropic state, with different rotational diffusion coefficients about the long and short axes that would account for the observed KWW functional form. Such motions are entirely different from the relaxation modes in the LC state where isotropic motions of the body become anisotropic due to the imposed anisotropic potential of the LC that is external to the mesogenic group. The effect of alignment on the relaxation characteristics in the LC state is shown in Figure 5, which depicts dielectric loss in the frequency domain (at 62 °C) measured on three different electrode surfaces. Both measured and deconvoluted spectra are shown. For clarity, the contribution due to dc conductivity is subtracted from the loss curve. Note the excellent isosbestic point, clearly visible at about 90 MHz, where permittivity is independent of macroscopic alignment. This, of course, tells us that eq 6 works pretty well. Deconvolution was carried out by assuming that the overall dielectric loss was composed of two CC. The results (Table 1) were consistent (independent of the type of alignment), suggesting that the overall loss could be represented by two relaxation processes. One remarkable observation is that the δ process decays exponentially; i.e., it can be described by the Debye equation. The α_m process, on the other hand, is much broader, with a CC β value of about 0.7. We note that the Debye-like dispersion has been reported for other LCMs[12,34] and SCLCPs.[10,16,35,36] It was speculated that since δ relaxation is associated with the end-over-end rotation of the mesogen, these motions must pass over 180° and are therefore likely to experience a rather uniform environment that is conducive to a Debye-like relaxation.

Quantitative evaluation of parameters S and μ_l^2/μ_t^2 can be made directly from dielectric measurements,[35,36] though a rigorous attempt at such calculation is difficult for several reasons. First, we have not measured the macroscopic order parameter S_d. And second (as pointed out by Attard and Williams[35,36]), the calculated parameter is very sensitive to the deconvolution of α_m and δ processes. Nonetheless, the following calculation was performed. On the basis of the observations from POM, we assumed that the sample measured on clean surfaces was homeotropic and that enabled us to estimate the macroscopic order parameter for the other two measurements. Making use of eqs 3, 4, and 6, the relaxation strength associated with the δ process in an arbitrarily aligned sample can be expressed as

$$\Delta\epsilon_{00}^{a} = \left(\frac{1 + 2S_d}{3}\right)\Delta\epsilon_{00}^{||} \qquad (8)$$

where superscripts a and || denote arbitrary and homeotropic alignment, respectively. By utilizing data in Table 1, we obtain the macroscopic order parameter S of −0.425 and −0.0536 for samples measured under the conditions specified as e and f, respectively, in Table 1.

Table 1. Fitting Results for LCM

	α			δ			α_m		
	$\Delta\epsilon$	τ (s)	β^a	$\Delta\epsilon$	τ (s)	β^b	$\Delta\epsilon$	τ (s)	β^b
isotropic[c]	9.35	1.5×10^{-9}	0.72						
LC (A)[d]				16.6	2.5×10^{-8}	1.0	1.5	4.4×10^{-10}	0.7
LC (B)[e]				0.83	2.7×10^{-8}	0.98	5.01	5.6×10^{-10}	0.69
LC (C)[f]				4.88	2.5×10^{-8}	0.98	4.10	6.0×10^{-10}	0.7

[a] KWW β parameter. [b] CC β parameter. [c] Measured at 90 °C. [d] Measured at 62 °C, clean copper electrodes. [e] Measured at 62 °C, PI-coated electrodes. [f] Measured at 62 °C, clean/PI-coated electrodes.

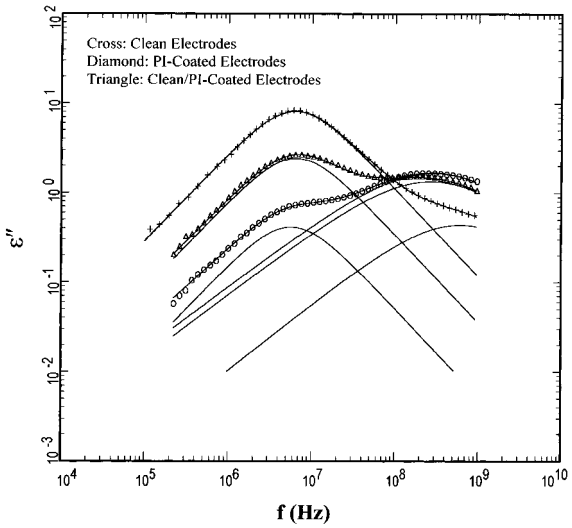

Figure 5. Dielectric loss in the frequency domain in the mesophase (at 62 °C) measured on three different electrode surfaces: clean copper electrodes (cross), PI-coated electrodes (circle), clean/PI-coated electrodes (triangle).

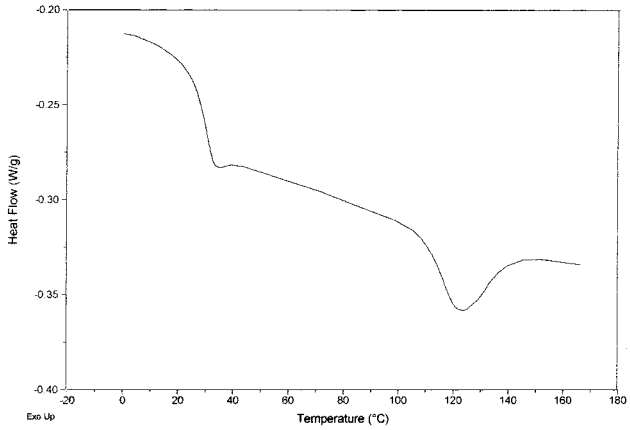

Figure 6. DSC thermogram of SCLCP.

The calculated values suggest that the alignment of samples under those specified conditions is very close to planar and random, respectively. It should be pointed out that the value of $S_d \approx 0$ (for sample specified as f in Table 1) does not automatically imply random alignment. $S_d \approx 0$ may also arise from the rotation of the local director from H (clean electrode) to P (PI-coated electrode) alignment. However, the dielectric response is identical in these two cases. The interesting question of what happens to relaxation dynamics when this LCM is attached to a polymer backbone was addressed next.

Side-Chain LC Polymer (SCLCP) Dynamics. The DSC thermogram of the SCLCP, shown in Figure 6, reveals a glass transition at 25 °C (onset temperature) and a phase transition at 122 °C, in agreement with the results reported in the literature.[19] Optical micrographs show a smectic texture below the clearing point. A characteristic batonnet pattern is observed at 122 °C, just below the T_i (Figure 7A), and the texture becomes more complex at lower temperature (Figure 7B).

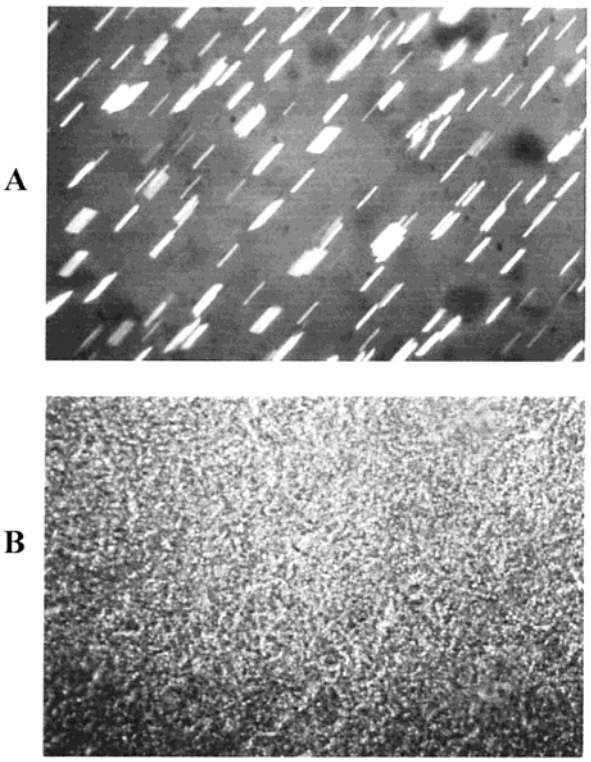

Figure 7. Polarized optical micrographs of SCLCP: (A) at 122 °C; (B) at 50 °C.

The relaxation behavior of this SCLCP is similar to that of the LCM and is also strongly influenced by the surface treatment of the electrodes. H-alignment is favored when clean copper electrodes are used, while P-alignment is promoted on the PI-treated surfaces. Dielectric loss in the frequency domain with temperature as a parameter is shown in parts A and B of Figure 8 for the measurements on clean and PI-treated electrode surfaces, respectively. Note that the loss spectra of Figure 8 cover 10 decades of frequency and a wide range of temperature in which our sample is in isotropic, liquid crystalline, and glassy state. Data in Figure 8A are examined first. The α process, characteristically skewed at high frequency, is observed above T_i. The loss peak broadens on approaching the I−S transition, as can be seen in the spectrum obtained at 125 °C in Figure 8A. Below T_i, the loss spectrum is characterized by a dominant, narrow δ process and a broad dispersion at high frequency due to the α_m process. A different pattern is observed in Figure 8B in the LC state. Here, the strength of the δ process is decreased, while that of the α_m process is increased. A common feature to both sets of data (Figure 8A,B) is the apparent merging of δ and

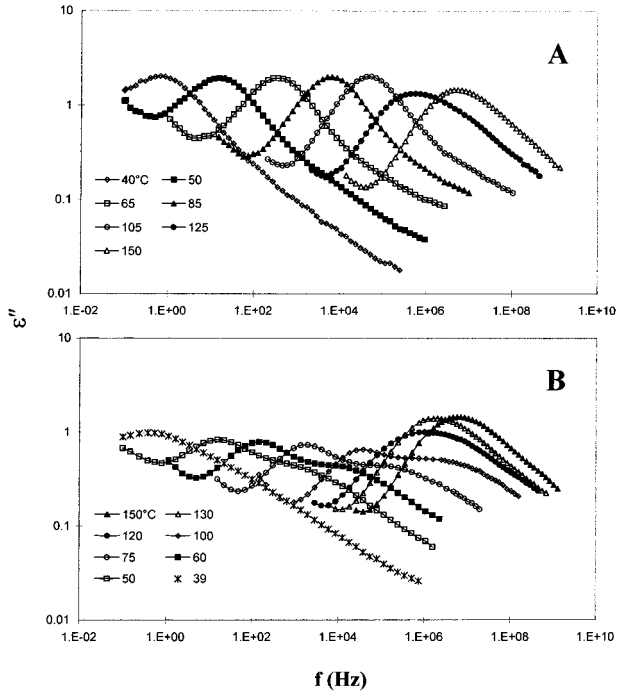

Figure 8. Dielectric loss in the frequency domain with temperature as a parameter for SCLCP: (A) clean copper electrodes; (B) PI-coated electrodes.

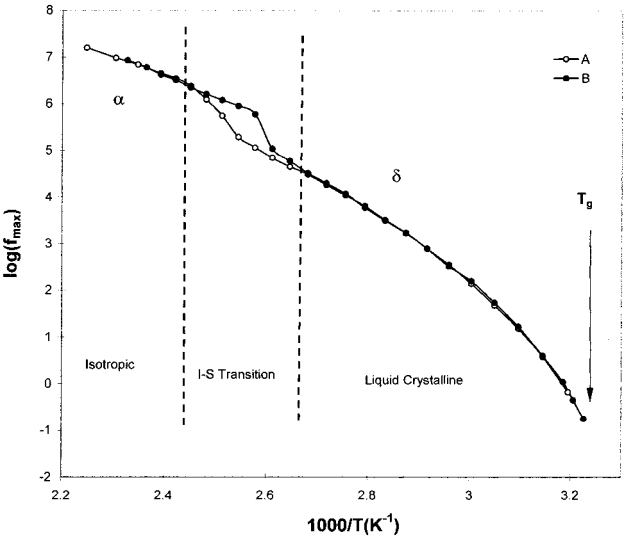

Figure 9. Frequency at maximum loss as a function of reciprocal temperature for α and δ processes in SCLCP.

α_m processes on approaching the T_g. We shall revert to this observation later in the text.

A plot of the frequency of maximum loss for different relaxations as a function of reciprocal temperature is shown in Figure 9 (letters A and B in Figure 9 correspond to those in Figure 8). To facilitate the presentation and discussion of these results, we subdivide Figure 9 into three regions: isotropic, transition (I−S), and liquid crystalline. It was anticipated that the relaxation time for the α process in the isotropic state would not be affected by the surface treatment and that was experimentally confirmed—all data in the isotropic region fall on top of each other. A more complex picture emerges in the LC state. As previously shown in Figure 8A, the α_m process is very broad, and it is difficult to identify the loss peak maximum in the measured spectra. Of course, the frequency of maximum loss could be determined by deconvolution of the overall loss, but that is not straightforward in the case of the α_m process and we shall address this issue later. Therefore, the data in the LC region of Figure 9 for samples A and B represent the δ process. It is clear that the relaxation time for the δ process is also independent of alignment, suggesting a common relaxation mechanism. The temperature dependence of the relaxation time is non-Arrhenius; the observed curvature bears a typical signature of cooperativity and glass transition. In this sense the δ process resembles the α process in glass formers, the difference in their molecular origin notwithstanding.

Next, we focus attention on the quantitative aspects of various relaxations and begin by considering the shape of the α process in the isotropic state. The α process is well described by the KWW function. The best fit KWW β parameter of 0.5 is found, in agreement with the value commonly found for most amorphous polymers but much lower than the value of 0.7, obtained for the LCM. The dielectric response of the SCLCP is dominated by the reorientation of the mesogenic groups because the dipole moment along the mesogenic group is much greater than in the siloxane backbone, and hence the decrease of the KWW β parameter (vis-à-vis the LCM) may be attributed to two factors: (1) coupling between the side chain and the backbone motions and (2) increased complexity (heterogeneity) of the relaxing environment (similar observation was made regarding relaxations in the LC state).

Let us now examine in more detail the relaxation characteristics in the LC state. We have shown above (Figure 8) that δ and α_m processes in the LC state are partially overlapped and separated by about 2 decades on the frequency (time) scale. Difficulties associated with resolving multiple relaxation processes were pointed out by Attard and Williams,[35,36] and additional information is often required to execute a meaningful deconvolution. The complexity associated with such endeavor is clear when one considers, for example, that the overall dielectric loss contains contributions from two relaxations, each of which is described by a HN function and each requiring four adjustable parameters: relaxation strength, relaxation time, and two shape parameters. Too much uncertainty is associated with the deconvolution based upon eight (two HN functions) parameters, and hence we had to look for a simplified yet physically meaningful solution. Careful inspection of the loss spectra over a wide range of frequency and temperature confirmed that the δ process was symmetric and narrow and hence could be described by only three parameters (for $\alpha = 1$, the HN equation reduces to the CC equation). An extensive fitting procedure showed that the use of the HN function to describe the α_m process yielded only a marginal improvement over the CC function. We then proceeded with deconvolution by assuming two CC equations, and these results are summarized in Table 2. Note that deconvolution was limited to the data in the temperature range between 105 and 75 °C. Below that temperature, α_m and δ processes merge (see Figure 8) to form a very broad dispersion. The implication is that the coupling between various molecular motions is no longer negligible, resulting in a physically unsound deconvolution. We shall revert to this issue shortly, but first we will set the stage for the forthcoming argument by reviewing the data in Table 2. The following relaxation characteristics of our SCLCP are independent of

Table 2. Fitting Results for SCLCP

		δ			α_m		
T (°C)	sample[a]	$\Delta\epsilon$	τ (s)	β^b	$\Delta\epsilon$	τ (s)	β^b
105	A	4.80	3.6×10^{-6}	0.87	0.89	6.8×10^{-8}	0.44
	B	0.94	3.7×10^{-6}	0.88	2.96	6.6×10^{-8}	0.44
100	A	4.83	5.6×10^{-6}	0.86	0.88	9.1×10^{-7}	0.44
	B	1.04	6.1×10^{-6}	0.87	2.79	8.7×10^{-8}	0.43
95	A	4.86	9.1×10^{-6}	0.85	0.86	1.5×10^{-7}	0.44
	B	1.12	1.0×10^{-5}	0.87	2.64	1.3×10^{-7}	0.43
90	A	4.90	1.6×10^{-5}	0.85	0.84	1.9×10^{-7}	0.44
	B	1.22	1.7×10^{-5}	0.85	2.52	2.0×10^{-7}	0.43
85	A	4.98	2.8×10^{-5}	0.83	0.81	2.3×10^{-7}	0.44
	B	1.33	3.1×10^{-5}	0.84	2.39	3.2×10^{-7}	0.43
80	A	5.05	5.2×10^{-5}	0.83	0.78	5.2×10^{-7}	0.43
	B	1.43	5.7×10^{-5}	0.83	2.26	5.8×10^{-7}	0.44
75	A	5.10	9.6×10^{-5}	0.83	0.76	8.9×10^{-7}	0.43
	B	1.53	1.1×10^{-4}	0.82	2.19	1.0×10^{-6}	0.44

[a] A = clean copper electrodes, B = PI-coated electrodes. [b] CC β parameter.

alignment: (1) the overall dielectric loss can be resolved into two relaxation processes; (2) the CC β parameter remains constant for the α_m process and decreases slightly (but systematically) with decreasing temperature for the δ process; and (3) the relaxation strength of the δ process *increases* while that of the α_m process *decreases* with *decreasing* temperature. These observations are in agreement with the theory that predicts that the overall loss at a given temperature should be a weighted sum of δ and α_m processes. The CC β parameter for the δ process in the polymer is in the range from 0.82 to 0.88, which is broader than the Debye-like δ process observed in the LCM but narrower than the α process in amorphous polymers. Additionally, the CC β parameter decreases with decreasing temperature. Together, these observations imply that the δ process in the SCLCP combines the characteristics of δ relaxation in the LCM (it is narrow) with the characteristics of α dynamics in amorphous polymers (it is cooperative). An increase in cooperativity with decreasing temperature is envisioned as a result of the enhanced coupling between molecular motions that give rise to the α_m process and those that contribute to the δ process. Since the latter is considerably slower, it acts as the limiting factor in determining the relaxation rate. This accounts for the apparent increase in the relaxation strength of the δ process and a simultaneous decrease in the relaxation strength of the α_m process. This trend becomes more pronounced as the temperature approaches T_g, and various motions become more highly interlocked.

We have referred throughout the text to the extensive work by Attard, Williams, and their group on similar SCLCPs,[35,36] and since we have largely built upon their studies, a comparison with their results is in order. In general, the relaxation characteristics of these two SCLCPs are quite similar. Attard and Williams found that the overall dielectric loss could be deconvoluted into two processes (δ and α_m) using two Fuoss−Kirkwood (FK) empirical functions.[37] (We note that both CC and FK functions give a symmetric dispersion and a similar, but not identical, spectral shape.[35,38]) They reported the FK β parameter of 0.85−0.88 for the δ process, very close to our values, and 0.34−0.36 for the α_m process, which is broader than in our sample. It is important to note that the spacer length in their samples (eight CH_2 groups) was considerably longer than in our sample (three CH_2 groups). Intuitively, one would assume that the decoupling of the motions associated with the mesogens from those of the backbone would be facilitated by increasing the spacer length, resulting ultimately in the relaxation similar to that of the LCM. But that was not found; the observed similarities in the relaxation characteristics of our SCLCPs suggest that the spacer length is not a crucial factor in determining the relaxation behavior.

We have also shown that the temperature dependence of the δ process is nonlinear. It is now of interest to examine how (and if) this behavior differs from that of a typical glass-former. It is well-known that the temperature dependence of the α process in polymers can be described by the Vogel−Fulcher−Tammann (VFT) or the Williams−Landel−Ferry (WLF) equation, which are mathematically equivalent. But despite the ability to describe most (though not all) glass-formers by the VFT (or WLF) equation, the deviation from the Arrhenius behavior is different for different materials. Over the years, various schemes have been proposed in search for a method for obtaining a unique fingerprint or signature of the $\tau(T)$ behavior of a material, so that different materials may be quantitatively compared and the parameters extracted from such a method related to materials characteristics. Since a single indexing parameter is desired, scalings such as T/T_g are introduced to condense the parameters into one. These indices are generally referred to as fragility indices;[39,40] for the purpose of this discussion suffice it to say that to compare fragility indices of different materials, it is recommended to fix the VTF τ_0 at the attempt frequency value of 10^{-14} s. The temperature dependence of relaxation time for δ, α_m, and α processes is shown in Figure 10. The δ process (diamonds) is slower than the α_m process (circles), and the two are essentially parallel over a range of temperatures. A similar observation was reported by Attard et al.,[35] though the two processes are expected to coalesce as T_g is approached[36] because of an increase in cooperativity with decreasing temperature. We focus attention on the δ process because it persists over a wider range of temperature. Interestingly, our VFT fits were not good with τ_0 fixed at 10^{-14} s but were excellent when the three adjustable parameters were allowed to change freely. The solid line in Figure 10 represents the best fit. The fitting parameters are $\tau_0 = 5.9 \times 10^{-11}$ s, $B = 1395$ K, and $T_0 = 249.7$ K, and the extrapolated T_g at $\tau = 100$ s is 299 K, which agrees very well with the onset of T_g measured by DSC (ca. 25 °C). Recall that the α_m and the δ process were observed to merge (Figure 8) on approaching the T_g. The

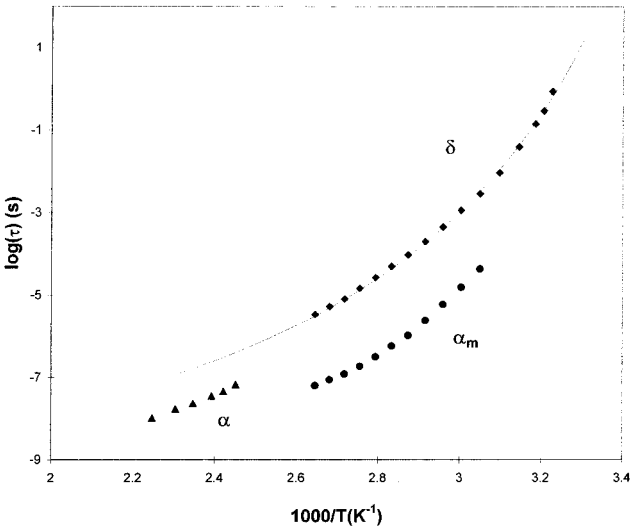

Figure 10. Relaxation time as a function of reciprocal temperature for α, α_m, and δ processes in SCLCP.

decoupling of molecular motions that underlie these two relaxations in the LC state slows down near T_g, where the rate of molecular motions is determined by the slower (rate limitng) δ process (in some sense this is analogous to the $\alpha-\beta$ splitting in isotropic liquids). We interpret this as evidence for the argument that the δ process governs the dynamics of SCLCPs near T_g, much like the α process does in the non-LC glass formers.

But while the VFT fits in Figure 10 are excellent, τ_0 is almost 4 decades slower than the attempt frequency value of 10^{-14} s. This unusual deviation is also clear in the WLF fits.[41] By setting $T^* = T_g = 25$ °C (obtained from DSC scan at 10 °C/min), we obtain an excellent fit to the WLF equation (dashed line in Figure 10) with $C_1 = 12.5$, $C_2 = 48.3$, and $\tau(T_g) = 210$ s. We observe that C_1 deviates considerably from the "universal" value of 16−17, while C_2 is close to its "universal" value and the relaxation time at T_g is very close to 100 s. As pointed out by Angell,[42] additional phenomena may be in play if the C_1 value is significantly different from 16 despite the fact that T_g is well referenced. We interpret this large deviation of C_1 from its "universal" value as a characteristics of the δ process that distinguishes this relaxations from those in non-LC glass formers.

Conclusions

We have completed a comprehensive study of the reorientational dynamics and macroscopic alignment in a LCM and a SCLCP synthesized and characterized in our laboratory. The principal conclusions are recapped as follows. In the isotropic state, the relaxation in LCM and SCLCP is well described by the KWW function and is independent of surface treatment. In the LC state ($T_i > T > T_c$), homeotropic (H) and planar (P) alignment can be promoted by an appropriate choice of the surface treatment of electrodes, and the overall dielectric response is a weighted sum of two separate dispersions, δ and α_m, that depend on the macroscopic alignment. The dielectric response is dominated by the slow process (δ) in the H-alignment while the fast process (α_m) becomes dominant in the P-alignment. The decoupling of various relaxation modes in the SCLCP diminishes gradually on approaching the T_g. The δ process governs the SCLCP dynamics near the T_g, much like the α process in the non-LC glass formers. Although the temperature dependence of the δ process can be well described by the WLF equation, it is distinguished from those in non-LC glass formers by a large deviation of C_1 from its universal value.

Acknowledgment. This material is based on work supported by the National Science Foundation under Grant DMR-9710480. The authors are grateful to Professor Graham Williams for many valuable comments and suggestions.

References and Notes

(1) Shibaev, V. P.; Plate, N. A. *Adv. Polym. Sci.* **1984**, *60/61*, 173.
(2) *Recent Advances in Liquid Crystalline Polymers*; Chapoy, L. L., Ed.; Elsevier: London, 1985.
(3) *Polymeric Liquid Crystals;* Blumstein, F., Ed.; Plenum Press: New York, 1985.
(4) *Side Chain Liquid Crystal Polymers*; McArdle, C. B., Ed.; Blackie and Son Ltd.: Glasgow, 1989.
(5) *Liquid Crystal Polymers: From Structure to Applications*; Collyer, A. A., Ed.; Elsevier. Appl. Sci.: London, 1992.
(6) *The Molecular Dynamics of Liquid Crystals;* Luckhurst, G., Veracini, C., Eds.; Kluwer Academic: Dordrecht, 1994.
(7) *Liquid Crystalline and Mesomorphic Polymers*; Shibaev, V. P., Lam, L., Eds.; Springer-Verlag: Berlin, 1994.
(8) Attard, G. S.; Araki, K.; Willams, G. *J. Mol. Electron.* **1987**, *3*, 1.
(9) Attard, G.; Araki, K.; Williams, G. *Br. Polym. J.* **1987**, *19*, 119.
(10) Araki, K.; Attard, G. S.; Kozak, A.; Williams, G.; Gray, G. W.; Lacey, D.; Nestor, G. *J. Chem. Soc., Faraday Trans. 2* **1988**, *84*, 1067.
(11) Kozak, A.; Moscicki, J. K.; Williams, G. *Mol. Cryst. Liq. Cryst.* **1991**, *201*, 1.
(12) Williams, G. In *The Molecular Dynamics of Liquid Crystals*; Luckhurst, G., Veracini, C., Eds.; Kluwer Academic: Dordrecht, 1994; Chapter 17, pp 431−450.
(13) Williams, G. *Chem. Soc. Rev.* **1972**, *72*, 55.
(14) Williams, G. In *Comprehensive Polymer Science*; Allen, G., Bevington, J. C., Eds.; Pergamon Press: London, 1988; Vol. 2, Chapter 18, pp 601−632.
(15) Cook, M.; Watts, D. C.; Williams, G. *Trans. Faraday Soc.* **1970**, *66*, 2503.
(16) Moscicki, J. K. In *Liquid Crystal Polymers: From Structure to Applications*; Collyer, A. A., Ed.; Elsevier. Appl. Sci.: London, 1992; Chapter 4, pp 143−236.
(17) Nordio, P. L.; Giorgio, R.; Segre, U. *Mol. Phys.* **1973**, *25*, 129.
(18) Williams, G.; Watts, D. C. *Trans. Faraday Soc.* **1970**, *66*, 80.
(19) Dishon, M.; Weiss, G. H.; Bendler, J. T. *J. Res. Natl. Bur. Stand.* **1985**, *90*, 27.
(20) Havrilliak, S.; Negami, S. *J. Polym. Sci., Part C* **1966**, *14*, 99.
(21) Ringsdorf, H.; Schneller, A. *Makromol. Chem., Rapid Commun.* **1982**, *3*, 557.
(22) Gemmell, P. A.; Gray, G. W.; Lacey, D. *Mol. Cryst. Liq. Cryst.* **1985**, *122*, 205.
(23) Gray, G. W.; Lacey, D.; Nestor, G.; White, M. S. *Makromol. Chem., Rapid Commun.* **1986**, *7*, 71.
(24) Williams, G. In *Keynote Lectures in Selected Topics of Polymer Science*; Riande, E., Ed.; CSIC: Madrid, 1997; Chapter 1, pp 1−40.
(25) Williams, G. In *Dielectric Spectroscopy of Polymeric Materials: Fundamentals and Application*; Runt, J. P., Fitzgerald, J. J., Eds.; American Chemical Society: Washington, DC, 1997; Chapter 1, pp 3−65.
(26) Simon, G. P. In *Dielectric Spectroscopy of Polymeric Materials: Fundamentals and Application*; Runt, J. P., Fitzgerald, J. J., Eds.; American Chemical Society: Washington, DC, 1997; Chapter 15, pp 329−378.
(27) Fitz, B.; Mijovic, J. *Macromolecules* **1999**, *32*, 3518.
(28) Fitz, B.; Andjelic, S.; Mijovic, J. *Macromolecules* **1997**, *30*, 5227.
(29) Andjelic, S.; Mijovic, J.; Bellucci, F. *J. Polym. Sci., Part B: Polym. Phys.* **1998**, *36*, 641.
(30) Pochan, J. M.; Fitzgerald, J. J.; Williams, G. In *Determination of Electronic and Optical Properties*, 2nd ed.; Rossitter, B., Baetzold, R. C., Eds.; Physical Methods of Chemistry Series; Wiley-Interscience: New York, 1993; Vol. VIII.

(31) Kranbuehl, D. E. In *Dielectric Spectroscopy of Polymeric Materials*; Runt, J. P., Fitzgerald, J. J., Eds.; American Chemical Society: Washington, DC, 1997; Chapter 13, pp 303−328.
(32) Kremer, F.; Arndt, M. In *Dielectric Spectroscopy of Polymeric Materials*; Runt, J. P., Fitzgerald, J. J., Eds.; American Chemical Society: Washington, DC, 1997; Chapter 15, pp 67−80.
(33) Mijovic, J.; Andjelic, S. *Macromolecules* **1996**, *29*, 239.
(34) Parneix, J. P. Thesis, Universite'de Lille I, France, 1984.
(35) Attard, G. S.; Williams, G. *Liq. Cryst.* **1986**, *1* (3), 253.
(36) Attard, G. S.; Araki, K.; Moura-Ramos, J. J.; Williams, G. *Liq. Cryst.* **1988**, *3* (6&7), 861.
(37) Fuoss, R. M.; Kirkwood, J. G. *J. Am. Chem. Soc.* **1941**, *63*, 385.
(38) McCrum, N. G.; Read, B. E.; Williams, G. *Anleastic and Dielectric Effects in Polymeric Solids;* Wiley: New York, 1967.
(39) Angell, C. A. In *Relaxations in Complex Systems*; Ngai, K. L., Wright, G. B., Eds.; National Technical Information Service; U.S. Department of Commerce: Springfield, VA, 1984; p 203.
(40) Green, J. L.; Ito, K.; Xu, K.; Angell, C. A. *J. Phys. Chem. B* **1999**, *103*, 3991.
(41) No further attempts were made to investigate the validity of the VFT equation over the whole range of temperature (and frequency): Stickel, F.; Fischer, E.; Richert, R. *J. Chem. Phys.* **1995**, *102*, 6251.
(42) Angell, C. A. *Polymer* **1997**, *38*, 6261.

MA0014158